Broadband Effective Permittivity Simulation and Measurement Techniques for 3-D-Printed Dielectric Crystals

Simon P. Hehenberger, *Graduate Student Member, IEEE*, Stefano Caizzone, *Member, IEEE*, Stefan Thurner, and Alexander G. Yarovoy, *Fellow, IEEE*

***Abstract*— Frequency-dependent dielectric properties of 3-D-printed structured dielectrics (dielectric crystals) with engineered effective permittivity for micro- and mmWave applications are studied. Different modeling and measurement techniques for broadband dielectric properties of such 3-D-printed crystals are reviewed, their tradeoffs discussed, and individual results compared. Numerically obtained results from the plane wave expansion method (PWEM) and Floquet port scattering are compared with traveling-wave measurements in both guided and free-space setups. Furthermore, the shortcomings of effective media theories (EMTs) and resonance measurement methods are addressed and contrasted against broadband methods. Individual simulation and measurement setups are reviewed with respect to dielectric crystals with simple cubic (SC) and face-centered cubic (FCC) symmetry, with different unit cell sizes and volumetric infill fractions. Extracted effective permittivity values from PWEM and Floquet port simulations show excellent agreement with traveling-wave measurements in both guided and free-space scenarios. Furthermore, the discussed broadband methods predict and measure frequency-dependent effects that are not covered by EMTs and resonance measurement setups, highlighting the necessity to adopt more sophisticated simulation tools for the design of graded-index devices. It is shown that the effective media bandwidth of dielectric crystals depends on the respective unit cell symmetry and that FCC symmetry obtains a significantly increased bandwidth compared with SC symmetry.**

***Index Terms*— 3-D-printing, additive manufacturing (AM), cutoff, dielectric crystals (DC), effective media, Floquet port, Maxwell–Garnett, periodic dielectric, permittivity measurement, permittivity modeling, plane wave expansion method (PWEM), structured dielectric.**

I. Introduction

DURING the last decade, the possibilities enabled by additive manufacturing (AM) exploded, and researchers increasingly tried incorporating the additional degrees of freedom offered by AM to design and manufacture new microwave components [1], [2]. Due to the cumbersome process of metalizing 3-D printed parts [3] and the large cost and bad surface quality of additive manufactured metal [4], many researchers have investigated all-dielectric approaches to create high-frequency devices. The ability to create complex shapes and periodic structures with different volumetric fill fractions of some base materials is used to create composites with engineered permittivity, further referred to as dielectric crystals (DC). AM is especially well-suited to introduce spatial variation to the volumetric infill fraction of a DC, which allows the creation of graded-index (GRIN) devices with engineered heterogeneous permittivity. This allows to introduce additional degrees of freedom in the design of dielectric resonator antennas [5], [6] [7], [8], [9], lenses [10], [11], substrates [12], and dielectric frequency-selective surfaces [13]. The successful design of DCs and subsequent GRIN devices requires solid knowledge of the constituent materials' permittivities, both as bulk medium and as a function of volumetric infill fraction. Furthermore, it is necessary to ensure that the DC behaves like an effective material over the desired bandwidth of operation. Due to the periodic nature of DCs, a natural cutoff frequency arises where the propagating wave will experience internal scattering, resulting in nonlinear dispersion. In literature, a commonly used approximation is that the unit cell should be ten times smaller than the smallest applied wavelength [7]. However, a more detailed study of this upper cutoff frequency is missing in the relevant literature. Generally, modeling and measurement techniques used to design and characterize DCs often rely on effective media theories (EMTs) and resonance measurement setups which are ill-suited to predict complex dispersion of EM waves in periodic media. Individual works have used more sophisticated methods to model the broadband effective permittivity of DCs. The PWEM is used in [14] to predict the permittivity tensor of a uniaxial anisotrop DC. Furthermore, Floquet port scattering simulations in combination with the Nicholsol–Ross–Weir method is used in [9] to model anisotropic permittivity. However, no comprehensive discussion of the different techniques together with a comparison to different measurement techniques has been attempted yet.

This work intends to address this gap and investigates frequency-dependent effective material parameters of additive-

Manuscript received 20 December 2022; revised 20 February 2023; accepted 3 March 2023. Date of publication 30 March 2023; date of current version 5 October 2023. *(Corresponding author: Simon P. Hehenberger.)*

Simon P. Hehenberger and Stefano Caizzone are with the Department of Communication and Navigation, German Aerospace Center (DLR), 82234 Wessling, Germany (e-mail: simon.hehenberger@dlr.de).

Stefan Thurner is with the Department of Microwaves and Radar, German Aerospace Center (DLR), 82234 Wessling, Germany.

Alexander G. Yarovoy is with the Department of Microwave Sensing, Signals and Systems, Technische Universiteit Delft, 2628 CD Delft, The Netherlands.

Color versions of one or more figures in this article are available at https://doi.org/10.1109/TMTT.2023.3259479.

Digital Object Identifier 10.1109/TMTT.2023.3259479

manufactured dielectric crystal lattices via several independent computational and experimental techniques. The effect of unit cell geometry, symmetry, and material on the effective permittivity is studied over a large frequency range up to effective media cutoff and beyond. Special attention is given to the effective media upper cutoff frequency of the individual DCs. It is worth highlighting that although the discussed techniques have been used and reported on independently, no comprehensive comparison of their respective predictions and discussion of their limitations and tradeoffs have been published yet. The presented techniques can be applied to study effects of different crystal symmetries, effective material bandwidths, and dispersion characteristics of DCs and GRIN devices.

This contribution is structured as follows. Section II justifies the need for broadband modeling of dielectric crystals and introduces the PWEM and Floquet port scattering simulations as valuable techniques for predicting the broadband behavior of dielectric crystals. The broadband simulation methods are contrasted against the Maxwell–Garnett approximation (MGA) for several dielectric crystals with simple cubic (SC) and face-centered cubic (FCC) symmetry, different unit cell sizes, and volumetric infill fractions. Section III gives insight into resonance, guided wave, and free-space wave measurement methods and discusses the differences and tradeoffs of the respective techniques concerning their capability of extracting the relative permittivity of DCs as a function of frequency. Representative setups for each measurement method are used to extract the effective permittivity of DCs with SC and FCC symmetry, different unit cell sizes, and infill fractions. Furthermore, the extracted effective permittivities from measurements are compared with the results from the various simulation techniques discussed in Section II. Section IV discusses the presented work and results, while Section V provides a conclusion and suggestions for future research work.

II. Modeling of Effective Material Parameters

In this work, we consider unit cells of different sizes, volumetric infills, and crystal symmetries created from a single material with relative permittivity $\varepsilon_{r,i}$ against the background of free space. The cells under investigation are generated via the method introduced in [15] and discussed in [16], which uses superimposed spatial harmonics along the reciprocal lattice vectors of the desired symmetry to create the geometry. The volumetric infill δ_i of the cells is controlled via the inversely proportional related threshold parameter th. Examples of generated cells in SC and FCC symmetry together with a plot of the volumetric infill as a function of the threshold parameter are depicted in Fig. 1. In the following, we first provide reasoning for the necessity of using broadband modeling and simulation techniques for DCs and further introduce different methods to compute the DCs' effective permittivity $\varepsilon_{r,eff}$ as a function of frequency and effective media cutoff. We study the effect of lattice constant a, threshold th, base material permittivity $\varepsilon_{r,i}$, and unit cell symmetry. The results from the broadband methods are summarized and contrasted against predictions obtained from MGA and summarized in Table I.

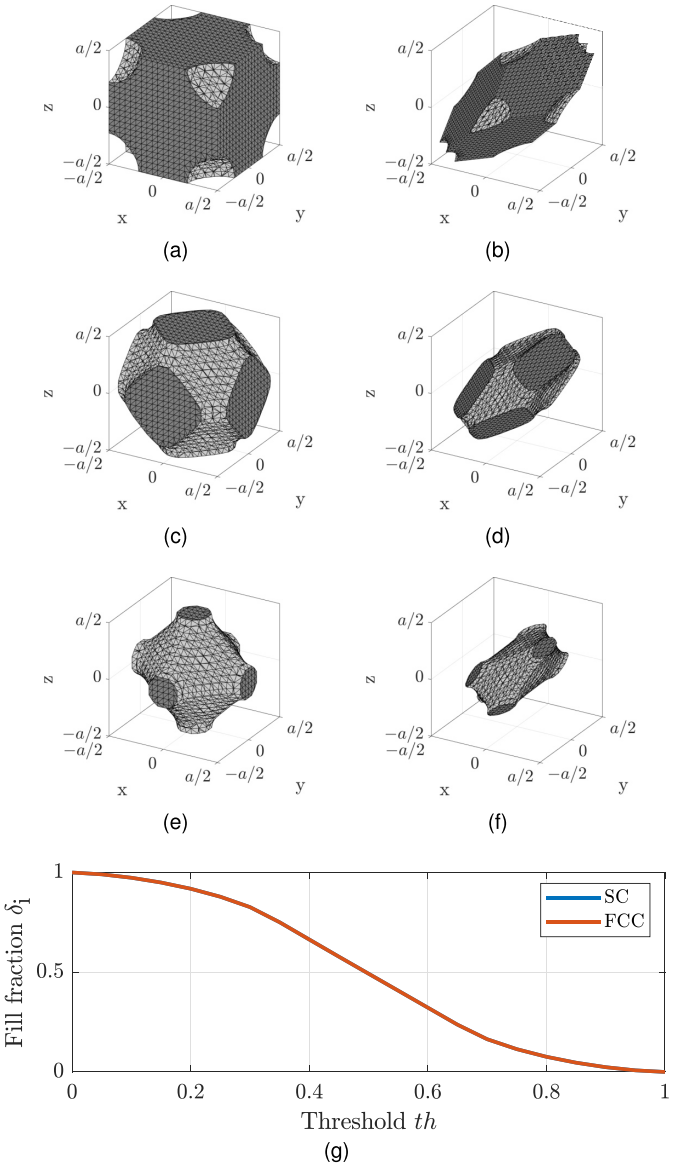

Fig. 1. Unit cells created by thresholding superimposed spatial harmonics in the direction of the reciprocal lattice vectors of the respective SC and FCC crystal geometries. SC unit cells (a) th = 0.2, (c) th = 0.4, (e) th = 0.6, and FCC unit cells (b) th = 0.2, (d) th = 0.4, (f) th = 0.6, and (g) their volumetric fill fraction as a function of the thresholding th parameter.

A. Necessity of Broadband Modeling

Consider the simplest case of electromagnetic (EM) wave propagation, a plane wave propagating through a linear, homogeneous, isotropic, and lossless material with permittivity ε and permeability μ, for which the H-field is written as

$$\mathbf{H} = \mathbf{H_0} e^{J(\mathbf{k}\cdot\mathbf{r}-\omega t)} \tag{1}$$

with ω representing the angular frequency, $\mathbf{k} = k\hat{\mathbf{k}}$ denoting the wave vector, and $\mathbf{H_0}$ is some constant vector in the plane orthogonal to $\mathbf{k}$. Plugging this field into Maxwell's equations, one obtains a relationship between frequency and wave vector [17]

$$k = \frac{\omega}{c_0} = \omega\sqrt{\varepsilon\mu} \tag{2}$$

TABLE I

COMPARISON OF SIMULATION RESULTS FOR THE EFFECTIVE PERMITTIVITY $\varepsilon_{R,EFF}$ AND EFFECTIVE MEDIA CUTOFF FREQUENCY f_C FOR DIELECTRIC CRYSTALS WITH DIFFERENT LATTICE CONSTANTS a, THRESHOLDS TH, AND BASE MATERIAL PERMITTIVITY $\varepsilon_{R,I}$ OBTAINED WITH THE MGA, PWEM, AND FLOQUET PORT SIMULATION

Crystal parameters				MGA		PWEM			Floquet port	
	a in mm	th	$\varepsilon_{r,i}$	$\varepsilon_{r,eff}$	f_c in GHz	$\varepsilon_{r,eff}$ at ω_n	ω_n	f_c in GHz	$\varepsilon_{r,eff}$ at 2 GHz	f_c in GHz
SC	10	0.35	4	$2.80 + \jmath 0.019$	-	3.07	0.067	7.82	$3.15 + \jmath 0.021$	8.34
SC	10	0.35	9	$4.61 + \jmath 0.025$	-	6.36	0.067	5.17	$6.53 + \jmath 0.046$	5.75
SC	10	0.5	4	$1.98 + \jmath 0.009$	-	2.20	0.067	7.64	$2.28 + \jmath 0.011$	9.73
SC	10	0.5	9	$2.68 + \jmath 0.008$	-	3.93	0.067	5.23	$4.12 + \jmath 0.024$	6.99
SC	7.5	0.35	4	$2.80 + \jmath 0.019$	-	3.07	0.05	10.43	$3.15 + \jmath 0.021$	11.12
SC	7.5	0.35	9	$4.61 + \jmath 0.025$	-	6.36	0.05	6.89	$6.53 + \jmath 0.046$	7.59
SC	7.5	0.5	4	$1.98 + \jmath 0.009$	-	2.20	0.05	10.19	$2.28 + \jmath 0.011$	12.88
SC	7.5	0.5	9	$2.68 + \jmath 0.008$	-	3.93	0.05	6.98	$4.16 + \jmath 0.024$	9.39
FCC	10	0.35	4	$2.68 + \jmath 0.018$	-	3.01	0.067	11.21	$3.15 + \jmath 0.021$	16.69
FCC	10	0.35	9	$4.29 + \jmath 0.021$	-	6.13	0.067	7.30	$6.49 + \jmath 0.047$	11.34
FCC	10	0.5	4	$1.98 + \jmath 0.009$	-	2.12	0.067	13.78	$2.21 + \jmath 0.011$	22.00
FCC	10	0.5	9	$2.68 + \jmath 0.008$	-	3.61	0.067	8.60	$3.89 + \jmath 0.027$	15.54
FCC	7.5	0.35	4	$2.68 + \jmath 0.018$	-	3.01	0.05	16.27	$3.15 + \jmath 0.021$	22.24
FCC	7.5	0.35	9	$4.29 + \jmath 0.021$	-	6.13	0.05	9.74	$6.49 + \jmath 0.047$	15.24
FCC	7.5	0.5	4	$1.98 + \jmath 0.009$	-	2.12	0.05	18.38	$2.21 + \jmath 0.011$	29.14
FCC	7.5	0.5	9	$2.68 + \jmath 0.008$	-	3.61	0.05	11.46	$3.89 + \jmath 0.027$	20.71

called the dispersion relationship. Now assume an EM wave traveling through an inhomogeneous periodic dielectric crystal where the permittivity is a function of space and takes on the form $\varepsilon(\mathbf{r}) = \varepsilon(\mathbf{r} + \mathbf{R})$, where $\mathbf{R}$ is a linear combination of the crystals' primitive lattice vectors. According to the Bloch theorem, the wave traveling through a periodic media can be described via [18]

$$\mathbf{H} = \mathbf{S}(\mathbf{r}) e^{\jmath(\boldsymbol{\beta}\cdot\mathbf{r} - \omega t)} \tag{3}$$

where $\mathbf{S}(\mathbf{r})$ is a periodic function with the same periodicity as the crystal and $\boldsymbol{\beta}$ is the Bloch vector [equivalent to the wave vector $\mathbf{k}$ as in (1)]. Due to the now periodic (inhomogeneous) nature of the medium the wave is propagating in, there is no simple solution for the dispersion relationship as for the homogeneous media in (2). Solutions need to be found by solving the wave equation

$$\nabla \times \left(\frac{1}{\varepsilon(\mathbf{r})} \times \mathbf{H}(\mathbf{r}) \right) = \left(\frac{\omega}{c_0} \right)^2 \mathbf{H}(\mathbf{r}) \tag{4}$$

which for the given Bloch vectors can be formulated as an eigenvalue problem with the eigenvalues $((\omega/c_0))^2$ corresponding to the eigenmodes $\mathbf{H}(\mathbf{r})$. Most works dealing with additive manufactured dielectric crystals do not consider the complex nature of the dispersion in periodic media but assume that the material can be modeled as a homogeneous effective media with linear dispersion according to (2). However, this assumption does only hold for sufficiently large wavelengths. As the frequency of the propagating fundamental mode in the lattice increases and its wavelength shrinks with respect to the lattice constant a, this assumption falls apart, implying an upper cutoff frequency for the effective medium approximation in the DC.

B. Maxwell–Garnett Effective Media Approximation

EMTs are the algebraic formulas with which the effective permittivity of composites and mixtures can be calculated. One effective media theory, commonly used for modeling the effective permittivity of additive-manufactured structured dielectrics, is the MGA. It models the very idealized case of a two-component mixture with spherical inclusions of relative permittivity $\varepsilon_{r,i}$ and volume fraction δ_i, in a host medium with relative permittivity $\varepsilon_{r,m}$. The MG rule gives the algebraic relationship for the effective permittivity of the mixture as [19]

$$\frac{\varepsilon_{r,eff} - \varepsilon_{r,m}}{(\varepsilon_{r,eff} + 2\varepsilon_{r,m})} = \delta_i \frac{\varepsilon_{r,i} - \varepsilon_{r,m}}{(\varepsilon_{r,i} + 2\varepsilon_{r,m})}. \tag{5}$$

Despite reports that the MG rule lacks accuracy at higher volume fractions [20], it has been used successfully to predict effective permittivities of DCs [16] and GRIN devices [21]. Fig. 2 displays the relationship between the computed effective permittivity $\varepsilon_{r,eff}$ for an SC and FCC unit cell. The unit cell consists of material with relative permittivity $\varepsilon_{r,i} \in [4,\ 9]$ and loss tangent $\tan\delta = 0.01$, in a host media $\varepsilon_{r,m} = 1$ (free-space). The MGA is not suitable to predict any broadband material characteristics, and more complex numerical methods must be used to model dielectric crystals' dispersion accurately. Numerical values for the computed effective permittivity are listed and compared with the results obtained from PWEM and Floquet port simulation in Table I.

C. Plane Wave Expansion Method

The PWEM is an efficient Fourier space technique to solve (4) with periodic boundary conditions with low to moderate dielectric contrast as an eigenvalue problem [22]. The PWEM computes the modes (eigenvectors) that fit the phase boundary condition imposed by the chosen Bloch vector $\boldsymbol{\beta}$ and their

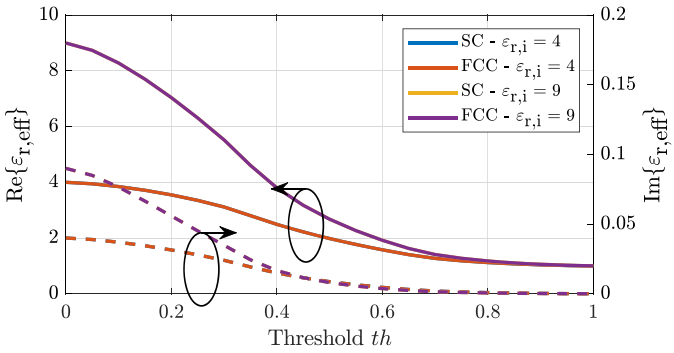

Fig. 2. Effective relative permittivity of SC and FCC dielectric crystals with $\varepsilon_{r,i} \in [4,\ 9]$ and loss tangent $\tan\delta = 0.01$ as a function of th obtained via the MGA.

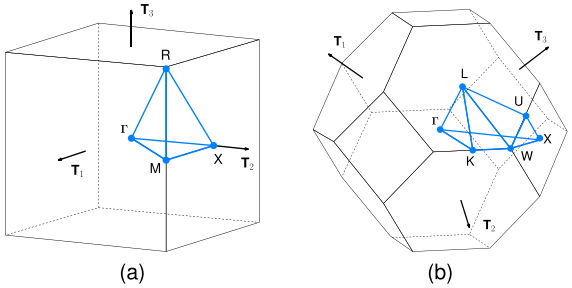

Fig. 3. Brillouin zones of (a) SC and (b) FCC crystals with visualization of the IBZ and its respective key points of symmetry.

respective wave numbers k_0 (eigenvalues). A complete analysis of the crystal with this method requires a dense sampling of the Bloch vectors in the Brillouin zone of the crystal, which is computationally demanding. Therefore, the PWEM is usually evaluated for the Bloch vectors on a path between the key points of symmetry, around the boundary of the irreducible Brillouin zone (IBZ) of the crystal as depicted in Fig. 3 [23]. The results of this reduced analysis are usually presented via band diagrams that display the eigenfrequencies of the individual modes as a function of the Bloch vector around the IBZ. The band diagram with the first ten modes for a unit cell with SC and FCC symmetry, created via $N = 3$ spatial harmonics and a threshold of th $= 0.5$, is depicted in Figs. 4(a) and 5(a), respectively, together with the light line of the fundamental mode. The light line represents the dispersion of the crystal if it is made from homogenous material with the effective material parameters exhibited by the periodic crystal geometry.

The fundamental modes for both the SC and FCC lattice show a linear dispersion characteristic for low-magnitude Bloch vectors (around the Γ key point of symmetry) as assumed by EMTs. However, for increasing Bloch vector magnitudes and wavelengths approaching the size of the unit cell, the assumption of linear dispersion for the dielectric crystal does not hold. In the band diagram, this is visible via the divergence of the bands from the light line. We arbitrarily define a normalized cutoff frequency $\omega_{n,c}$, for which the divergence with respect to the light line is less than 1%. Frequencies below $\omega_{n,c}$ are shaded in green in Figs. 4(a) and 5(a), respectively. For the case of linear dispersion, the effective

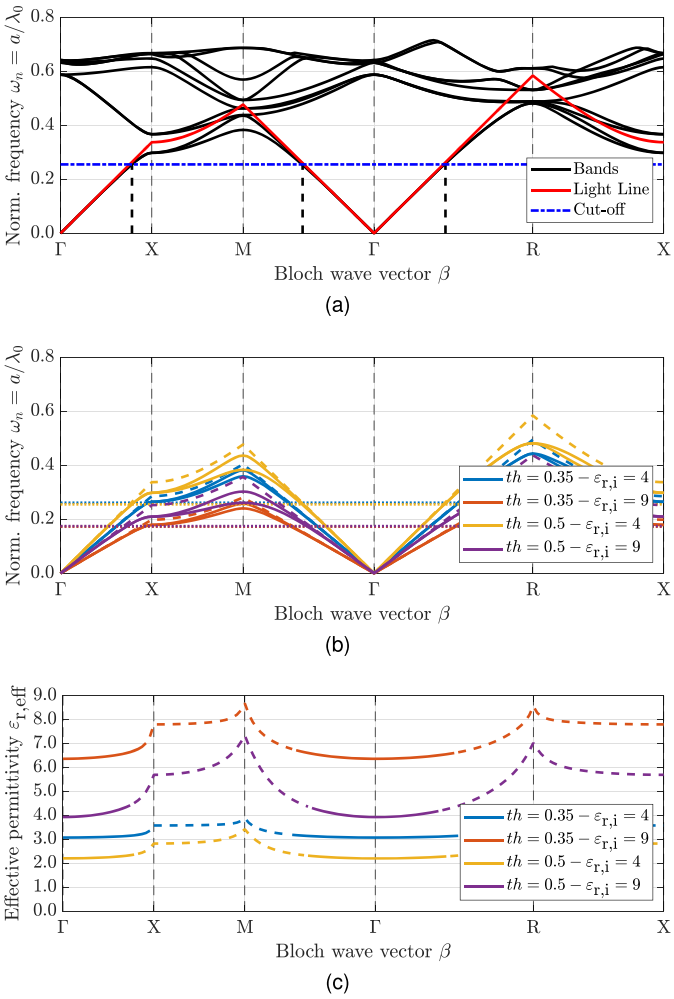

Fig. 4. Simulation of dielectric crystals with SC symmetry via the PWEM method. (a) Band diagram $\varepsilon_{r,i} = 9$, th = 0.5. (b) Fundamental modes of SC dielectric crystals with different $\varepsilon_{r,i}$ and volumetric infill fractions th. (c) Extracted relative permittivities from results in (b).

material refractive index n_{eff} can be extracted from the slope of the dispersion curve via

$$n_{\mathrm{eff}} = \frac{|\boldsymbol{\beta}|}{k_0} = \sqrt{\varepsilon_{r,\mathrm{eff}}\mu_r} \tag{6}$$

which for purely dielectric media ($\mu_r = 1$) is the square root of the effective relative permittivity. The effect of crystal permittivity and the threshold is studied via the fundamental modes of SC and FCC dielectric crystals with thresholds th $\in [0.35, 0.5]$ and $\varepsilon_{r,i} \in [4, 9]$ together with their respective light lines (dashed lines), and normalized cutoff frequencies (dotted lines) that are plotted in Figs. 4(b) and 5(b), respectively. Furthermore, their effective permittivities, computed via (6), are displayed in Figs. 4(c) and 5(c), respectively, and effective permittivity values represented with solid lines indicate values where the linear dispersion approximation gives less than 1% error. Already within the arbitrarily defined effective media theory cutoff of 1% divergence from the light line, one can observe a drastic change in the effective permittivity values. An interesting observation is the increased cutoff frequency of the linear dispersion in the FCC crystal at $\omega_{n,c} \approx 0.4$, compared with the SC crystal where the cutoff already appears

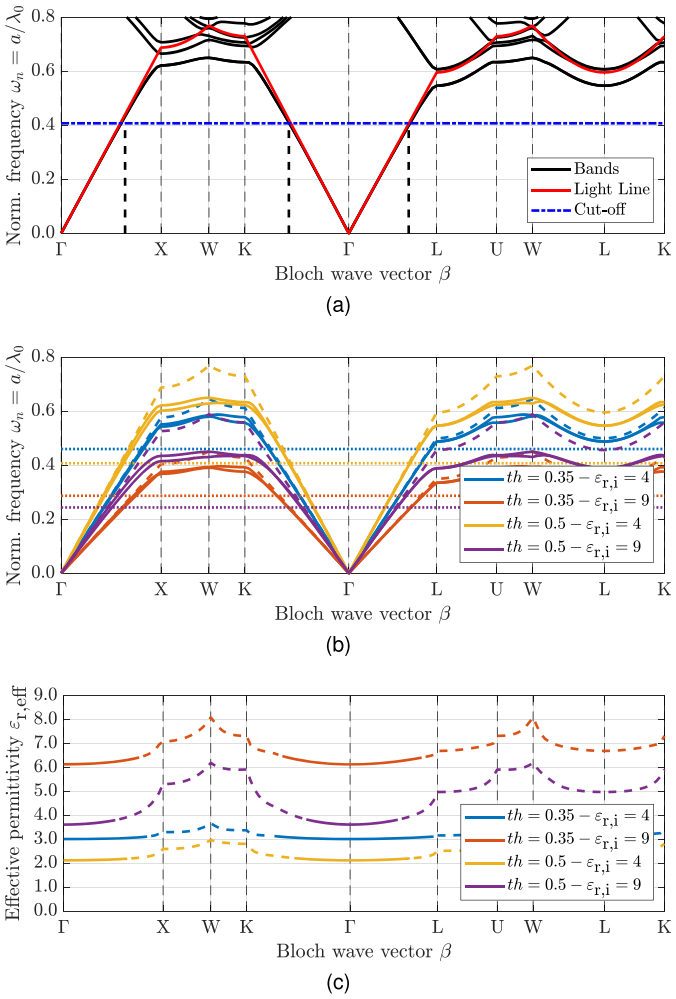

Fig. 5. Simulation of dielectric crystals with FCC symmetry via the PWEM method. (a) Band diagram $\varepsilon_{r,i} = 9$, th $= 0.5$. (b) Fundamental modes of FCC dielectric crystals with different $\varepsilon_{r,i}$ and volumetric infill fractions th. (c) Extracted relative permittivites from results in (b).

at $\omega_{n,c} \approx 0.25$. Generally, the cutoff is shifted to lower normalized frequencies for increasing values of the dielectric crystal material permittivity $\varepsilon_{r,i}$ and decreasing thresholds th (increasing volumetric infill fraction). This observation can be explained by the higher effective permittivity of the dielectric crystal $\varepsilon_{r,eff}$ for increasing $\varepsilon_{r,i}$ and decreasing th, and the resulting shorter wavelength of a wave propagating in the crystal. The unit cell size does not influence the shape and behavior of the bands with respect to the normalized frequency. Numerical values for the estimated cutoff frequency and extracted effective permittivity for a normalized frequency corresponding to 2 GHz are listed and compared with the results obtained from MGA and Floquet port simulation in Table I.

D. Floquet Scattering

While the PWEM is a useful tool, approximations of 3-D infinite lattices and plane waves are difficult to approximate in experimental setups. A widely used method to circumvent this problem when dealing with the characterization of periodic structures is to compute the scattering of a 2-D infinite slab

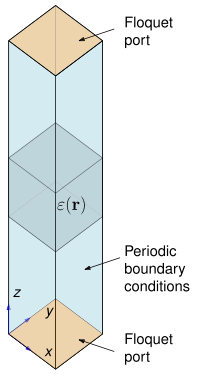

Fig. 6. Schematic of a Floquet port simulation of a dielectric unit cell with inhomogeneous permittivity $\varepsilon(\mathbf{r})$.

via a Floquet port simulation. Modeling the material in terms of reflection and transmission parameters is favorable because these quantities are relatively easy to obtain with real-world measurement setups. For the simulation, the unit cell is set up with periodic boundary conditions along two axes and Floquet excitation along the third, as depicted in Fig. 6. This setup allows the simulation of scattering of a semi-infinite slab of the material under test (MUT) with variable angles of incident and polarization. Based on the scattering parameters S_{11} and S_{21}, one is able to extract effective parameters based on the Nicholson–Ross–Weir (NRW) method [24], [25]. Although the NRW method can extract both complex permittivity and permeability of an MUT, the extraction of both complex quantities causes ill-behavior of the procedure at frequencies corresponding to one-half wavelength in the sample [26]. As this work only deals with dielectric materials, the assumption $\mu_r = 1$ is generally imposed on the used NRW procedure. The definition of all-dielectric materials leads to a more accurate and stable computation of the MUT's complex permittivity [26]. Floquet port simulations have been carried out for SC and FCC crystals with $\varepsilon_{r,i} \in [4,\ 9]$ and loss tangent $\tan\delta = 0.01$, thresholds th $\in [0.35,\ 0.5]$, and unit cell sizes $a \in [7.5\text{ mm},\ 10\text{ mm}]$. The unit cells in simulations were oriented such that the wave is propagating along the $\Gamma - X$ direction. The scattering parameters from simulations have been used to compute the effective material permittivity $\varepsilon_{r,eff}$ which are displayed for the different crystal symmetries and unit cell sizes in Figs. 7 and 8 respectively. For all the simulations, a constant effective permittivity is observed for lower frequencies. However, at higher frequencies, resonances start to appear in the extracted effective permittivity values, corresponding to the cutoff frequency where the effective media approximation breaks down. Generally, one is able to observe a much-increased cutoff for FCC crystals which is in accordance with the observations in the previous section, where the behavior of the crystal was studied via the PWEM method. Furthermore, the same conclusions as from the PWEM investigation about the effect of crystal permittivity $\varepsilon_{r,i}$ and threshold th can be drawn from the Floquet port simulations. The cutoff shifts to lower frequencies for higher $\varepsilon_{r,i}$ and lower th (higher volumetric infill). In addition, the effect of the unit cell size is clearly visible as it does not change

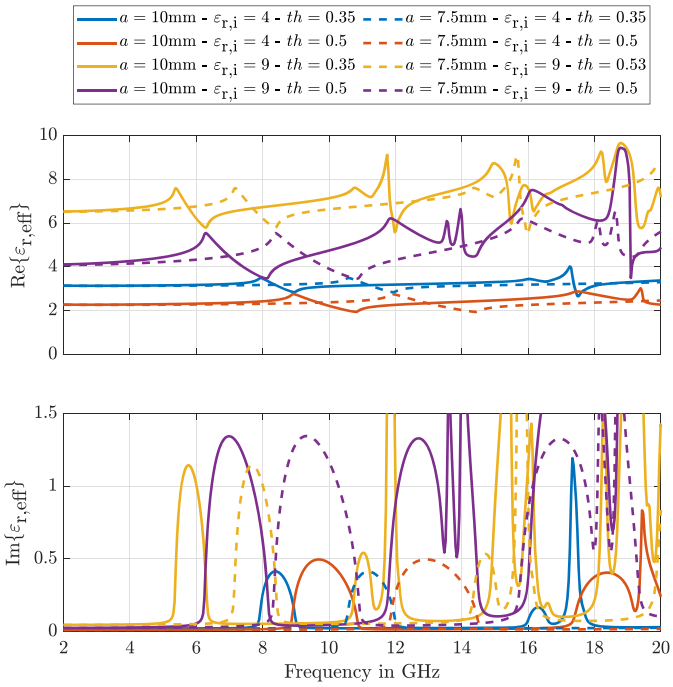

Fig. 7. Effective permittivity values of SC dielectric crystals with different material permittivities $\varepsilon_{r,i}$ and thresholds th for unit cell sizes 10 mm (solid lines) 7.5 mm (dashed lines), computed with the NRW method adapted for non-magnetic materials.

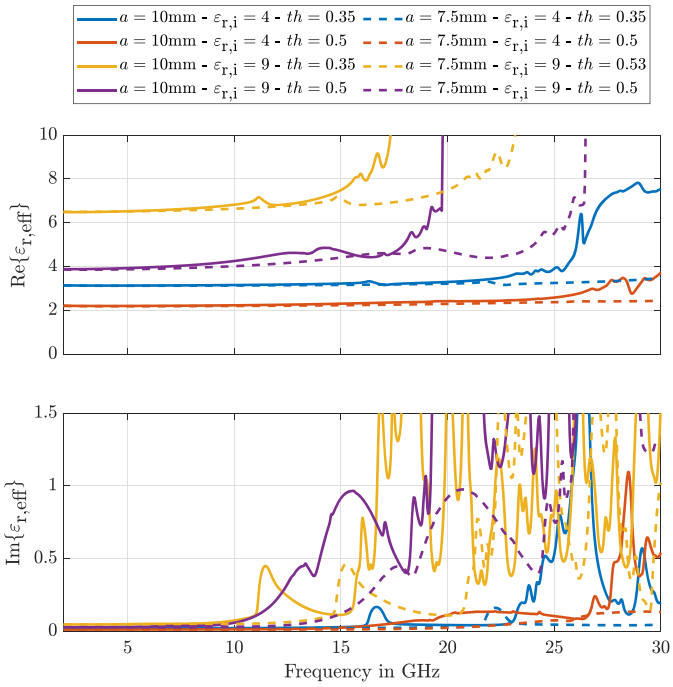

Fig. 8. Effective permittivity values of FCC dielectric crystals with different material permittivities $\varepsilon_{r,i}$ and thresholds th for unit cell sizes 10 mm (solid lines) 7.5 mm (dashed lines), computed with the NRW method adapted for non-magnetic materials.

the values or behavior of the extracted material parameters but only shifts them in frequency. Numerical values for the estimated cutoff frequency and computed effective permittivity are listed and compared with the results obtained from MGA and the PWEM method in Table I.

E. Comparison of Simulation Methods

To give a better overview of the results of the individual simulation methods, the results with respect to computed permittivity and estimated effective media theory cutoff frequency are summarized in Table I. Effective permittivity values obtained from the Floquet port simulations are displayed for the lowest simulation frequency of 2 GHz. To compare effective permittivity values obtained via the PWEM to the results extracted from the Floquet port simulations, the values are computed at normalized frequencies ω_n corresponding to 2 GHz. The effective media cutoff frequency f_c is computed from the PWEM results with the 1% divergence point from the light line. For the Floquet port results, the effective media cutoff frequency is determined via the local maximum of the imaginary part of the effective permittivity at the first visible resonance.

While the results obtained via the PWEM and Floquet port simulations agree reasonably well with each other, one can observe a rather large discrepancy with respect to the results obtained via the MGA method. The error in the results obtained with the MGA method seems to be worse with decreasing threshold th or increasing volumetric fill fraction, which is an effect also observed in [20]. The obtained cutoff frequencies agree reasonably well with each other for the SC crystals. However, they show significant disagreement for FCC crystals where the Floquet port simulation shows very high cutoff frequencies. However, this issue can be explained by the ill-suited definition of the cutoff frequency in the Floquet port simulations via the local maxima of the effective permittivities' imaginary part. This definition was chosen for simplicity because these were easily identifiable. A more suitable definition of the cutoff shall be investigated in future work.

III. Measurement Methods

In general, the measurement of dielectric material parameters proves to be quite difficult. The field encompasses many measurement techniques for different frequencies and material types. There are several tradeoffs to consider when selecting a measurement approach, and an excellent overview of the topic is given in [27]. Two classes of measurement approaches suitable for high-frequency characterization can be distinguished: resonator and traveling-wave techniques. Resonance methods are generally used for measuring the loss of low-loss dielectrics. They work by placing an MUT in a resonator cavity and comparing the empty and filled cavity measurements. The material parameters are extracted based on the shift in resonance frequency and quality factor. Resonance methods can obtain very high resolution, especially for low-loss materials. However, they deliver results only at one frequency point in contrast to broadband measurement techniques [28]. Traveling-wave methods provide the main benefit of broadband material characterization and can further be distinguished into guided and free-space methods. While in guided wave methods, the MUT is inserted into a waveguide structure, in free-space approaches, the MUT is placed between two directive antennas. Both the methods rely on the

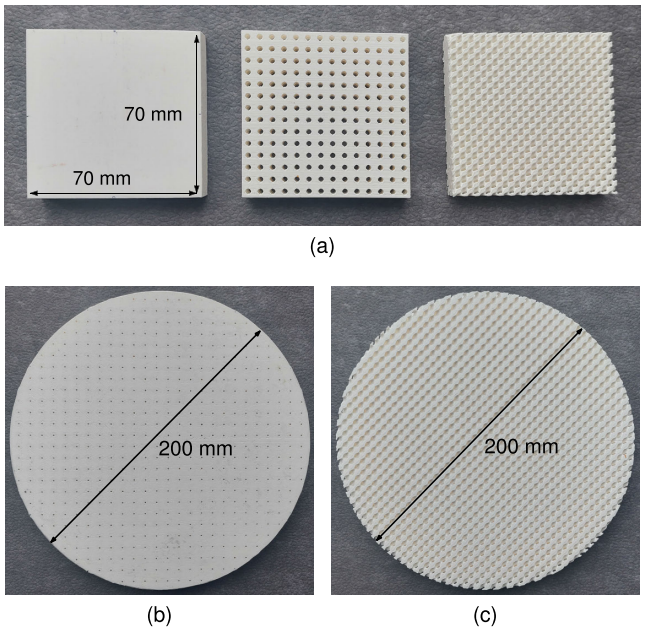

Fig. 9. Additively manufactured dielectric crystal samples for material characterization. (a) Sample for measurement in a suspended microstrip measurement system, from left to right: bulk sample, SC sample, and FCC sample. (b) SC sample and (c) FCC sample for characterization in a free-space traveling-wave setup.

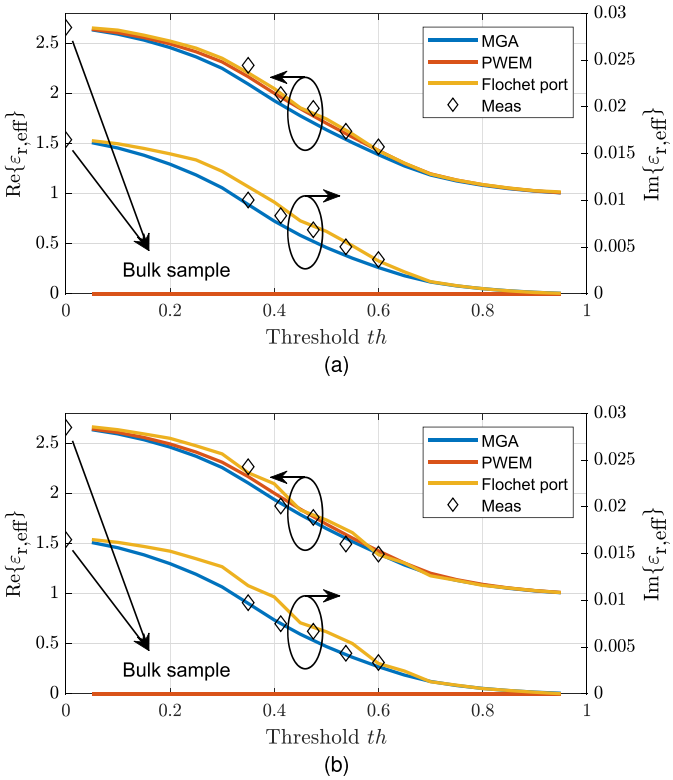

Fig. 10. Extracted effective permittivities of (a) SC and (b) FCC dielectric crystals with different thresholds obtained with a suspended microstrip resonator compared with the results obtained via the MGA, PWEM, and Floquet port simulations.

measurement of reflection and transmission coefficients from material samples and extract the material parameters based on the NRW method as introduced in Section II-D. They are not as well-suited to measure low-loss materials as resonance methods but provide the main benefit of delivering broadband results. In this work, we consider one experimental setup for the resonant, guided, and free-space methods, respectively, to characterize SC and FCC dielectric crystals with different threshold th and unit cell size a. The results are compared with predictions from the different simulation techniques discussed in Section II. Details and tradeoffs of the three individual setups are discussed below.

Manufacturing of measurement samples for all the methods is done with an Ultimaker 3 FDM AM machine using the Ultimaker white polylactic (PLA) filament. All the samples were manufactured with identical material and printing parameters[1] to ensure consistency of bulk material properties throughout the measurements. SC and FCC dielectric crystal samples are designed according to the method discussed in [16] with $N = 3$ spatial harmonics, with grating vectors equal to the individual reciprocal lattice vectors of the SC and FCC symmetries. Prior to measurements of dielectric crystal samples, printed bulk samples of the selected material were subjected to measurements with the resonative setup, and it was found that it obtained a relative permittivity of $\varepsilon_r = 2.66$ and a loss tangent of $\tan\delta = 0.0062$. Examples of the bulk, SC, and FCC samples used in the resonance and free-space traveling-wave setup are depicted in Fig. 9. Measurements were carried out with samples oriented such that propagating waves through the samples would travel along the $\Gamma - X$ path of the crystal.

[1]Layer height 0.15 mm; nozzle diameter: 0.4 mm; nozzle temperature: 195 °C; bed temperature: 60 °C; max. printing speed: 50 mm/s.

In the resonance measurement setup, the sample was oriented with the $\Gamma - X$ path normal to the microstrip ring resonator.

A. Resonance Setup

The resonance measurement setup used in this work is based on a suspended microstrip ring resonator which has already been introduced in [29] and used for the characterization of 3-D-printed dielectric crystals in [16]. Here, we use the resonant setup to test predictions about the effective permittivity obtained from the MGA theory, PWEM, and Floquet port simulations. For this, multiple lattices in SC and FCC with thresholds th $\in$ {0.35, 0.4125, 0.475, 0.5375, 0.6} were manufactured with a lattice constant of $a = 5$ mm in a cubic volume of $70 \times 70 \times 10$ mm^3. The extracted effective permittivity results for the individual samples at the resonance frequency of the system f_{res} are listed in Table II as well as plotted together with the simulation results as a function of th in Fig. 10 for SC and FCC samples, respectively. Care was taken that simulation results obtained via PWEM and Floquet port simulations are represented at frequency points corresponding to f_{res} of the measurements. Obviously, for PWEM data, no imaginary part of the effective permittivity is reported. While PWEM and Floquet port results show a better agreement with respect to the real part of the measured effective permittivity, the MGA theory produces more accurate results concerning the measured imaginary part. For the SC samples, the predictions by PWEM and Floquet port simulations agree with the measurements well while the relative

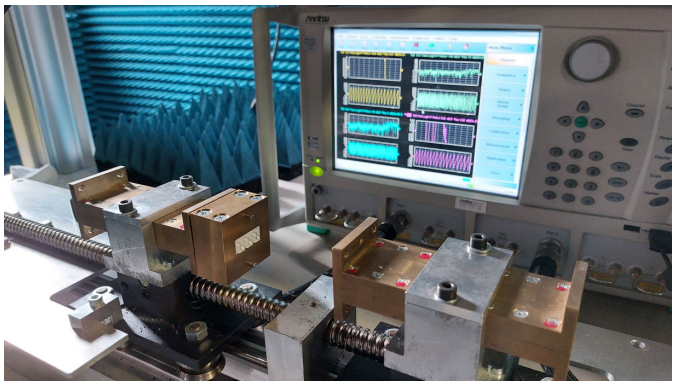

Fig. 11. Measurement setup for reflection and transmission measurements in rectangular waveguides.

permittivity values obtained with the MGA produce a larger error. For the FCC, no favorable simulation technique can be identified from the presented data.

B. Traveling-Guided Wave Setup

One option to circumvent the shortcomings of a resonance approach is to use a traveling-guided wave measurement system, where an MUT sample is fit into a waveguide and subjected to reflection and transmission measurements. This work uses a measurement system based on rectangular waveguides as depicted in Fig. 11. Prior to the measurement of material samples, the setup is calibrated using a through–reflect–line approach. The measurement is performed by inserting an MUT sample into the waveguide sample holder and recording transmission and reflection coefficients via a VNA. The effective material parameters are computed in postprocessing via the NRW method. Although traveling-guided wave setups are considered broadband, they are usually only used in the fundamental mode of the used waveguide. Therefore, this work makes use of several consecutive rectangular waveguide standards, as listed in Table III, to cover a wide frequency range. This implies a high effort as many different-sized samples needed to be machined with high precision, and individual calibrations for consecutive waveguide standards had to be carried out before measurement.

SC and FCC dielectric crystal samples were manufactured with two different thresholds th $\in$ [0.35, 0.5] and unit cell sizes $a \in$ [7.5 mm, 10 mm]. The initial samples were printed in the dimensions of the WR284 waveguide standard with a thickness of two unit cells. Samples for measurements in consecutively smaller waveguide standards, as listed in Table III, were cut from the original sample to reduce errors produced over multiple print jobs. Accurate machining of the MUT samples is essential since gaps between the sample and waveguide walls can cause significant errors in the extracted material parameters [30]. The precise machining is an error source that gets more significant with increasing frequency as the waveguide dimensions get consecutively smaller, but machining tolerances stay the same. Therefore, waveguide measurements were carried out up to 12.4 GHz, and the resulting extracted complex effective permittivities are plotted as a function of frequency in Figs. 12 and 13, respectively.

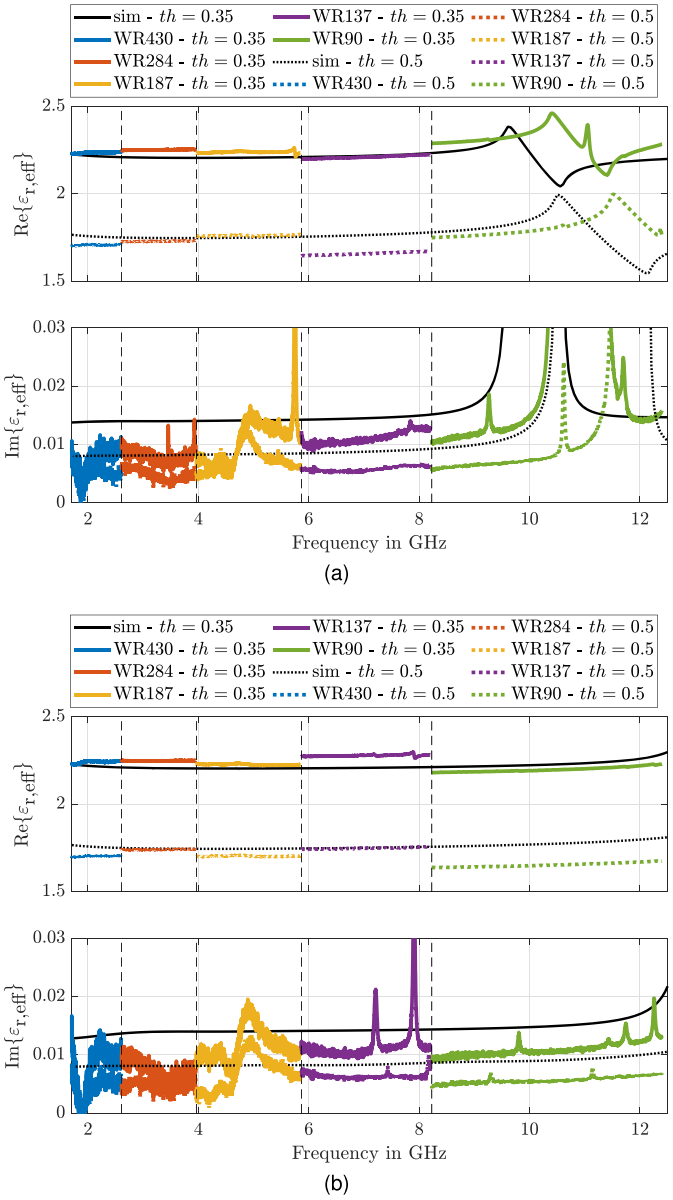

Fig. 12. Effective permittivities of dielectric crystal samples with SC symmetry, different unit cell sizes, and volumetric infills extracted from Floquet port simulations and measurements in consecutive rectangular waveguide standards via a modified NRW method. (a) $a = 10$ mm. (b) $a = 7.5$ mm.

Extracted permittivity values across consecutive waveguide standards show excellent agreement with each other and with the results obtained via the HFSS Floquet port simulations. The measurement of the SC sample with unit cell size $a = 10$ mm in Fig. 12(a) is especially interesting since the measurement frequency range covers the first resonance of the crystal lattice. Although the simulated and measured resonance peak shows a slight offset of about 1 GHz, the simulation accurately predicts the shape and size of the resonance peak in the measurement. One is able to observe several sharp peaks in the extracted imaginary part of the effective permittivity that is not predicted by simulations and is most likely caused by small manufacturing and machining imperfections.

TABLE II

CHARACTERIZATION OF ADDITIVELY MANUFACTURED DIELECTRIC CRYSTALS WITH SC AND FCC GEOMETRIES IN TERMS OF THEIR DIELECTRIC PERMITTIVITY AND LOSS TANGENT VIA A RESONANT MEASUREMENT SETUP COMPARED WITH PREDICTIONS OBTAINED VIA THE MGA, THE PWEM, AND FLOQUET PORT SCATTERING

Sample		MGA		PWEM	Floquet Port		Measurement		
Crystal	th	$\varepsilon_{r,eff}$	tanδ	$\varepsilon_{r,eff}$ at f_{res}	$\varepsilon_{r,eff}$ at f_{res}	tanδ	f_{res} in GHz	$\varepsilon_{r,eff}$	tanδ
BULK	-	-	-	-	-	-	1.441	2.66	6.2E-3
SC	0.35	2.17	4.6E-3	2.17	2.21	5.2E-3	1.515	2.28	4.4E-3
SC	0.4125	1.98	3.9E-3	1.96	2.00	4.7E-3	1.581	1.99	4.2E-3
SC	0.475	1.79	3.3E-3	1.77	1.80	4.0E-3	1.616	1.85	3.7E-3
SC	0.5375	1.62	2.7E-3	1.60	1.63	3.4E-3	1.680	1.62	3.1E-3
SC	0.6	1.45	2.0E-3	1.43	1.43	2.5E-3	1.729	1.47	2.5E-3
FCC	0.35	2.17	4.6E-3	2.14	2.21	5.2E-3	1.518	2.27	4.3E-3
FCC	0.4125	1.98	4.0E-3	1.93	2.03	4.8E-3	1.609	1.88	4.0E-3
FCC	0.475	1.79	3.3E-3	1.75	1.79	4.0E-3	1.640	1.76	3.8E-3
FCC	0.5375	1.62	2.7E-3	1.56	1.64	3.5E-3	1.720	1.50	2.9E-3
FCC	0.6	1.45	2.1E-3	1.40	1.39	2.3E-3	1.754	1.39	2.4E-3

TABLE III

RECTANGULAR WAVEGUIDE STANDARDS USED IN THIS WORK FOR EFFECTIVE PERMITTIVITY MEASUREMENT OF ADDITIVE MANUFACTURED DIELECTRIC CRYSTALS

WG	Frequency [GHz]	Width [mm]	Height [mm]
WR430	1.70 - 2.60	109.22	54.61
WR284	2.60 - 3.95	72.14	36.09
WR187	3.95 - 5.85	47.50	23.75
WR137	5.85 - 8.20	34.79	17.40
WR90	8.20 - 12.4	22.86	10.16

C. Traveling Free-Space Wave Setup

Another option to measure broadband material parameters is to use a free-space wave measurement system, where an MUT sample is placed between two directive antennas and subjected to reflection and transmission measurements. The experimental setup used in this work, as depicted in Fig. 14, consists of two horn antennas with wideband focusing lenses on opposite sides of a probe iris, surrounded by absorbing materials to avoid measurement artifacts due to scattering off of foreign objects. The system is calibrated via a line-reflect–line approach prior to measurements to compensate for the lens-spillover loss and other system errors. For measurement, the sample is fixed within the probe iris and is illuminated by EM radiation. The reflection and transmission parameters are recorded by a vector network analyzer and stored for postprocessing. Measurements in the Cx-, X-, Ku-, K-, and Ka-bands with different feed horns were carried out to cover a wide frequency range from 6 to 40 GHz. Four different dielectric crystal samples in SC and FCC geometry with two different thresholds th $\in$ [0.35, 0.5] and unit cell sizes $a \in$ [7.5 mm, 10 mm] were manufactured as cylindrical disks with a diameter of 200 mm and a thickness of two unit cells. The individual samples, fixed in the probe iris, were subjected to reflection and transmission measurements, and the resulting extracted effective permittivities are depicted as a function of frequency in Figs. 15 and 16, respectively. Measurements across consecutive frequency bands show excellent agreement with each other and with the simulation results obtained from the HFSS Floquet port simulations. Oscillations in the extracted permittivity values in the Cx-band are due to the measurement setup reaching a lower frequency limit. As the wavelength gets too large with respect to the used sample size, the diffraction effects around the sample start to play a significant role and distort the measurement. For SC samples, the first resonance's position, shape, and magnitude are accurately predicted by the HFSS Floquet port simulations. However, for frequencies above 25 GHz, some simulation artifacts are visible, especially in the data for the SC dielectric crystal with a unit cell size of $a = 10$ mm. The measurement of FCC crystals shows some minor deviations from simulated behavior; most notably, the FCC crystal with $a = 7.5$ mm exhibits a relatively strong resonance at around 30 GHz, which is not well predicted by simulations.

IV. DISCUSSION

It has been demonstrated that EMTs like the MGA provide good results for lower volumetric fill fractions and lower permittivity contrasts. However, they lack accuracy for high relative infill and moderate to high permittivity values. In addition, they lack the capability to predict any broadband behavior of graded dielectrics. Similar restrictions apply to dielectric characterization via resonance measurement setups. To address the limitations of EMTs and resonance measurement methods, two alternatives for both modeling and experimental verification are discussed in this work. For modeling and simulation of dielectric crystals, the PWEM and Floquet port simulations have been shown to be powerful tools for predicting the effective material parameters and broadband effects like cutoff frequencies in the graded materials. The PWEM gives insight into the EM behavior of an infinite lattice via computing the dispersion for a given wave vector through the lattice. However, the PWEM can be computationally demanding depending on the complexity of the unit cell and the number of wave vectors considered in the analysis. Furthermore, as a Fourier space technique, it suffers from the Gibbs phenomenon, which limits its accuracy for unit cells with high permittivity contrast. However, the insights provided by the PWEM are of tremendous value, not only for predicting the effective permittivity values of graded dielectrics but also

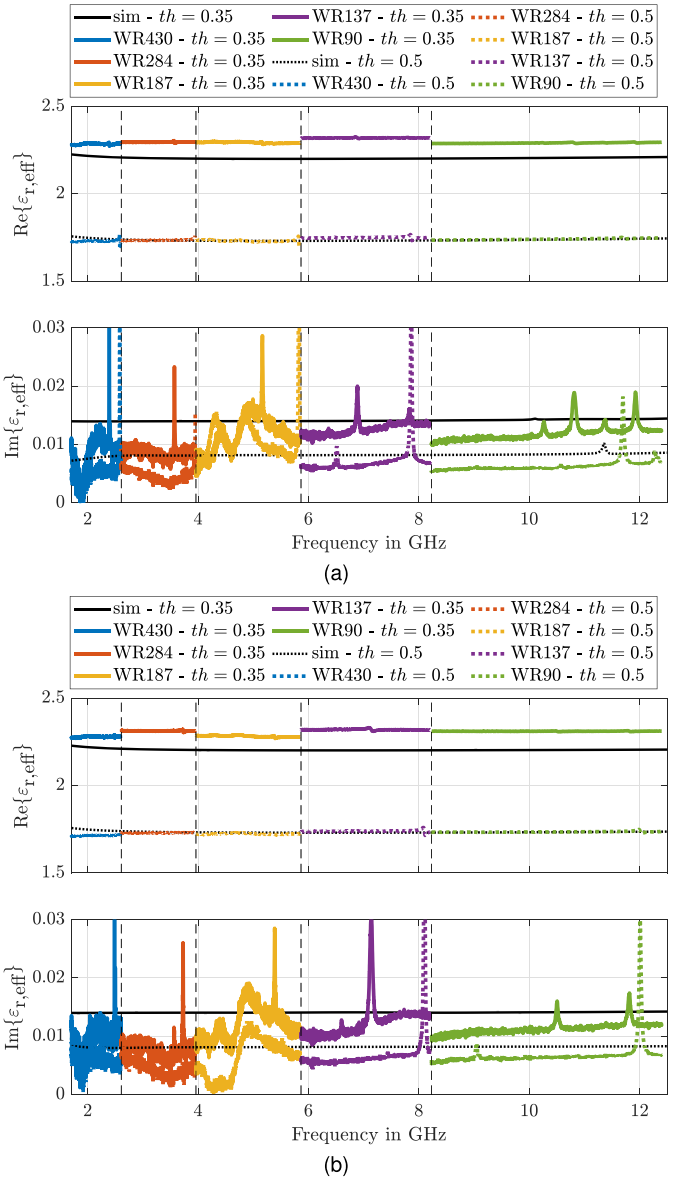

Fig. 13. Effective permittivities of dielectric crystal samples with face-centered symmetry, different unit cell sizes, and volumetric infills extracted from Floquet port simulations and measurements in consecutive rectangular waveguide standards via a modified NRW method. (a) $a = 10$ mm. (b) $a = 7.5$ mm.

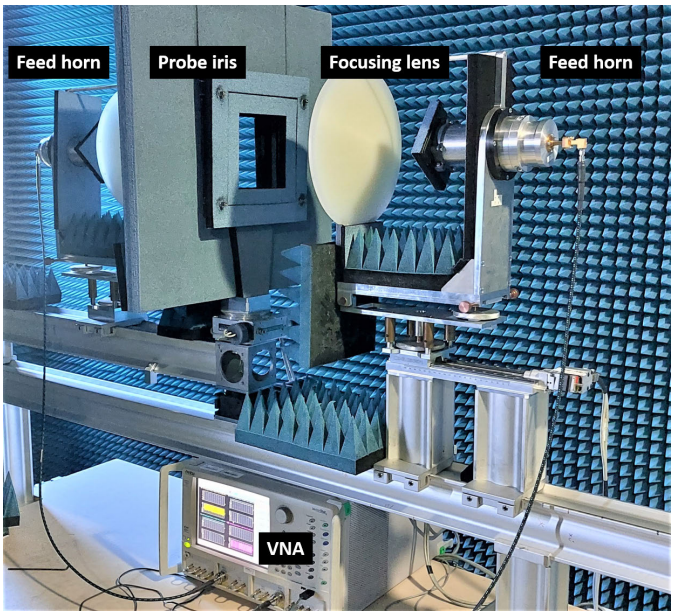

Fig. 14. Measurement setup for reflection and transmission measurements consisting of feed horn antennas with focusing lenses, connected to vector network analyzer, on opposite sides of a probe iris.

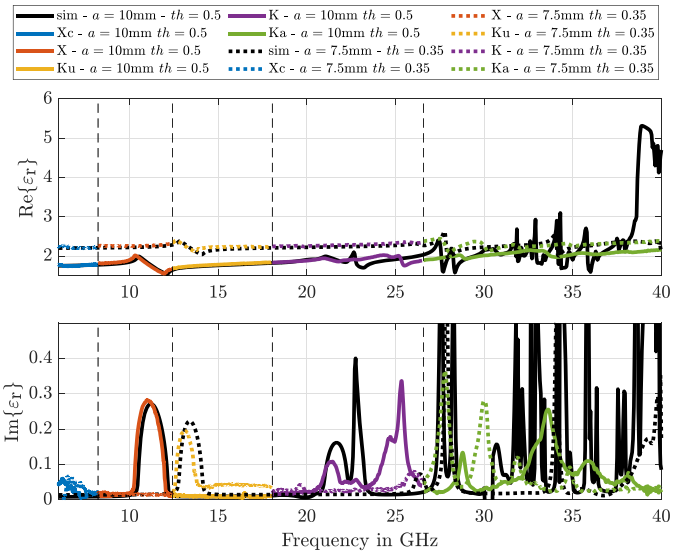

Fig. 15. Effective permittivity in real (top) and imaginary parts (bottom) extracted from free-space traveling-wave measurements of SC dielectric crystals with different unit cell size a and threshold th.

to study bandgaps and exotic dispersion effects such as self-collimation. Floquet port simulations have the main benefit of not considering the infinite lattice but modeling the scattering of a semi-finite slab of the MUT. The results of this scattering analysis are more easily comparable to the quantities obtained with real-world traveling-wave measurement equipment. For experimental verification, traveling-wave techniques in both a guided and a free-space setup have been used to confirm predictions on the broadband effective permittivity obtained from the PWEM and Floquet port simulations. While both the methods delivered results in satisfying agreement to simulations, several tradeoffs between the methods can be identified that are worth considering when selecting a measurement approach. The main drawback of the guided wave method is that the MUT samples need to be precisely machined to fit the cross section of the used waveguide, as small air gaps between the sample and waveguide walls can already cause significant errors in the retrieved material parameters. This issue of precise machining gets more significant with increasing frequency as the MUT sample size gets smaller while machining tolerances stay the same. A further drawback of guided wave methods is the inability to measure the same sample in different polarizations. The advantage, on the other hand, is the small sample size (with respect to the wavelength) necessary, which is especially beneficial for measurements at larger wavelengths (below 10 GHz). In contrast to the guided wave setup, the free-space method has the drawback that the sample needs to be quite large compared with the wavelength to limit the influence of diffraction effects in the measurement. Furthermore, a free-space measurement setup is more difficult to calibrate and needs more careful consideration

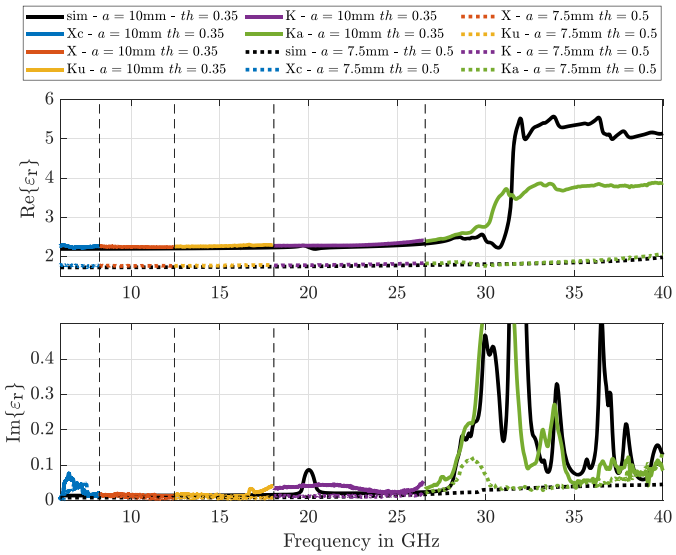

Fig. 16. Effective permittivity in real (top) and imaginary parts (bottom) extracted from free-space traveling-wave measurements of FCC dielectric crystals with different unit cell size a and threshold th.

of its environment, as radio sources or reflections from objects in the near vicinity can cause significant errors in the recorded scattering parameters. However, the free-space method bears the advantage that one sample of the MUT is sufficient to measure a wide frequency band and arbitrary polarizations planes.

V. Conclusion

This work presents novel insights into periodic dielectric structures (dielectric crystals), which are usually used to synthesize a wide range of relative permittivity values with varied volumetric infill in the design of GRIN devices. An investigation of the effect of different unit cell sizes, base material permittivity, volumetric infill, and crystal symmetry on the effective permittivity and upper cutoff frequency of the effective material bandwidth is presented. This is done by reviewing and applying different computational and experimental methods to extract frequency-dependent effective permittivity values over a wide range of samples and frequencies. It is worth emphasizing that although the discussed techniques have been used and reported on independently, no comprehensive comparison of results on comparable samples and discussion of their limitations and tradeoffs have been published yet. Predictions from the considered numerical methods agree excellently with extracted permittivities obtained via independent measurement methods. We demonstrate that the periodic nature of the engineered dielectric crystals results in an upper cutoff frequency above which the assumption of an effective media is not applicable. Furthermore, we show that this upper cutoff depends on the crystal's periodicity, volumetric infill, symmetry, and constituent materials. We conclude that the commonly used approximation, that unit cell size should be ten times smaller than the applied wavelength, is severely lacking. Generally, it is difficult to give a straightforward unit cell size to wavelength ratio as a design limit because such a limit depends on the used unit cell symmetry and the permissible dispersion in the desired material properties. Based on the presented work, several topics for future work are identified:

1) *Cut-off*: Simulation and measurement methods considered in this work clearly showed the existence of upper cutoff frequencies and their dependency on unit cell size, fill fraction, and crystal symmetry. However, no definition or detailed investigation of this upper cutoff has been carried out yet.
2) *Anisotropy*: Due to the nature of the AM process, (un-) intentional anisotropic material properties might arise that have yet to be investigated. The simulation and measurement methods discussed here can be extended to include polarization-dependent effects to model and experimentally verify the effective permittivity tensor of such dielectric crystals.
3) *Optimization*: The difference between the simple and FCC unit cells implies a considerable potential for further unit cell optimization in terms of bandwidth or linearity of the volumetric infill ratio concerning the threshold.

References

[1] E. S. Rosker, R. Sandhu, J. Hester, M. S. Goorsky, and J. Tice, "Printable materials for the realization of high performance RF components: Challenges and opportunities," *Int. J. Antennas Propag.*, vol. 2018, pp. 1–19, Jan. 2018, doi: 10.1155/2018/9359528.

[2] J. M. Jafferson, H. Vinu, and K. Sekaran, "A study of additive manufacturing technologies and metallizing techniques for microwave waveguide components," *Mater. Today, Proc.*, vol. 46, pp. 1328–1334, Jan. 2021, doi: 10.1016/j.matpr.2021.02.420.

[3] K. Lomakin et al., "3D printed slotted rectangular hollow waveguides," in *IEEE MTT-S Int. Microw. Symp. Dig.*, Boston, MA, USA, Jun. 2019, pp. 342–345, doi: 10.1109/MWSYM.2019.8700864.

[4] C. R. Garcia, R. C. Rumpf, H. H. Tsang, and J. H. Barton, "Effects of extreme surface roughness on 3D printed horn antenna," *Electron. Lett.*, vol. 49, no. 12, pp. 734–736, 2013, doi: 10.1049/el.2013.1528.

[5] A. A. Althuwayb et al., "3-D-printed dielectric resonator antenna arrays based on standing-wave feeding approach," *IEEE Antennas Wireless Propag. Lett.*, vol. 18, no. 10, pp. 2180–2183, Oct. 2019, doi: 10.1109/LAWP.2019.2939734.

[6] Z.-X. Xia, K. W. Leung, and K. Lu, "3-D-printed wideband multi-ring dielectric resonator antenna," *IEEE Antennas Wireless Propag. Lett.*, vol. 18, no. 10, pp. 2110–2114, Oct. 2019, doi: 10.1109/LAWP.2019.2938009.

[7] G. Mazingue, B. Byrne, M. Romier, and N. Capet, "3D printed ceramic antennas for space applications," in *Proc. 14th Eur. Conf. Antennas Propag. (EuCAP)*, Copenhagen, Denmark, Mar. 2020, pp. 1–5, doi: 10.23919/EuCAP48036.2020.9135312.

[8] Q. Lamotte et al., "Multi-permittivity 3D-printed ceramic dual-band circularly polarized dielectric resonator antenna for space applications," in *Proc. 15th Eur. Conf. Antennas Propag. (EuCAP)*, Dusseldorf, Germany, Mar. 2021, pp. 1–5, doi: 10.23919/EuCAP51087.2021.9411245.

[9] C. D. Morales, C. Morlaas, A. Chabory, R. Pascaud, M. Grzeskowiak, and G. Mazingue, "3D-printed ceramics with engineered anisotropy for dielectric resonator antenna applications," *Electron. Lett.*, vol. 57, no. 18, pp. 679–681, Aug. 2021.

[10] J. W. Allen and B.-I. Wu, "Design and fabrication of an RF GRIN lens using 3D printing technology," *Proc. SPIE*, vol. 8624, pp. 164–170, Mar. 2013, doi: 10.1117/12.2000708.

[11] J.-M. Poyanco, F. Pizarro, and E. Rajo-Iglesias, "Cost-effective wideband dielectric planar lens antenna for millimeter wave applications," *Sci. Rep.*, vol. 12, no. 1, p. 4204, Mar. 2022, doi: 10.1038/s41598-022-07911-z.

[12] S. Zhang, C. C. Njoku, W. G. Whittow, and J. C. Vardaxoglou, "Novel 3D printed synthetic dielectric substrates," *Microw. Opt. Technol. Lett.*, vol. 57, no. 10, pp. 2344–2346, Oct. 2015, doi: 10.1002/mop.29324.

[13] J. H. Barton, C. R. Garcia, E. A. Berry, R. G. May, D. T. Gray, and R. C. Rumpf, "All-dielectric frequency selective surface for high power microwaves," *IEEE Trans. Antennas Propag.*, vol. 62, no. 7, pp. 3652–3656, Jul. 2014, doi: 10.1109/TAP.2014.2320525.

[14] C. R. Garcia et al., "3D printing of anisotropic metamaterials," *Prog. Electromagn. Res.*, vol. 34, pp. 75–82, 2012.
[15] R. C. Rumpf and J. Pazos, "Synthesis of spatially variant lattices," *Opt. Exp.*, vol. 20, no. 14, pp. 15263–15274, Jun. 2012, doi: 10.1364/OE.20.015263.
[16] S. P. Hehenberger, A. P. T. Adithyababu, and S. Caizzone, "Effective permittivity measurement of 3D-printed dielectric crystals," in *Proc. 16th Eur. Conf. Antennas Propag. (EuCAP)*, Madrid, Spain, Mar. 2022, doi: 10.23919/EuCAP53622.2022.9769370.
[17] D. M. Pozar, *Microwave Engineering*, 4th ed. Hoboken, NJ, USA: Wiley, 2012. [Online]. Available: https://search.library.wisc.edu/catalog/9910153599402121
[18] J. D. Joannopoulos, S. G. Johnson, J. N. Winn, and R. D. Meade, *Photonic Crystals*. Princeton, NJ, USA: Princeton Univ. Press, 2008. [Online]. Available: http://ab-initio.mit.edu/book/
[19] V. A. Markel, "Introduction to the Maxwell Garnett approximation: Tutorial," *J. Opt. Soc. Amer. A, Opt. Image Sci.*, vol. 33, no. 7, p. 1244, Jul. 2016, doi: 10.1364/JOSAA.33.001244.
[20] M. I. Mishchenko, J. M. Dlugach, and L. Liu, "Applicability of the effective-medium approximation to heterogeneous aerosol particles," *J. Quant. Spectrosc. Radiat. Transf.*, vol. 178, pp. 284–294, Jul. 2016, doi: 10.1016/j.jqsrt.2015.12.028.
[21] A. Goulas et al., "Fused filament fabrication of functionally graded polymer composites with variable relative permittivity for microwave devices," *Mater. Des.*, vol. 193, Aug. 2020, Art. no. 108871, doi: 10.1016/j.matdes.2020.108871.
[22] K. Brakora, C. Barth, and K. Sarabandi, "A plane-wave expansion method for analyzing propagation in 3D periodic ceramic structures," in *Proc. IEEE Antennas Propag. Soc. Int. Symp.*, Washington, DC, USA, Jul. 2005, pp. 192–195, doi: 10.1109/APS.2005.1551971.
[23] W. Setyawan and S. Curtarolo, "High-throughput electronic band structure calculations: Challenges and tools," *Comput. Mater. Sci.*, vol. 49, no. 2, pp. 299–312, Aug. 2010, doi: 10.1016/j.commatsci.2010.05.010.
[24] A. M. Nicolson and G. F. Ross, "Measurement of the intrinsic properties of materials by time-domain techniques," *IEEE Trans. Instrum. Meas.*, vol. IT-19, no. 4, pp. 377–382, Nov. 1970, doi: 10.1109/TIM.1970.4313932.
[25] W. B. Weir, "Automatic measurement of complex dielectric constant and permeability at microwave frequencies," *Proc. IEEE*, vol. 62, no. 1, pp. 33–36, Jan. 1974, doi: 10.1109/PROC.1974.9382.
[26] J. Baker-Jarvis, E. J. Vanzura, and W. A. Kissick, "Improved technique for determining complex permittivity with the transmission/reflection method," *IEEE Trans. Microw. Theory Techn.*, vol. 38, no. 8, pp. 1096–1103, Aug. 1990, doi: 10.1109/22.57336.
[27] R. N. Clarke et al., "A guide to the characterisation of dielectric materials at RF and microwave frequencies," Inst. Meas. Control, London, U.K., Tech. Rep., 2003. [Online]. Available: https://eprintspublications.npl.co.uk/2905/
[28] K. Y. You, *Materials Characterization Using Microwave Waveguide System*. Rijeka, Croatia: InTech, 2017, doi: 10.5772/66230.
[29] I. Waldron and S. N. Makarov, "Measurement of dielectric permittivity and loss tangent for bulk foam samples with suspended ring resonator method," in *Proc. IEEE Antennas Propag. Soc. Int. Symp.*, Albuquerque, NM, USA, Jul. 2006, pp. 3175–3178, doi: 10.1109/APS.2006.1711285.
[30] S. B. Wilson, "Modal analysis of the 'gap effect' in waveguide dielectric measurements," *IEEE Trans. Microw. Theory Techn.*, vol. MTT-36, no. 4, pp. 752–756, Apr. 1988, doi: 10.1109/22.3581.

Simon P. Hehenberger (Graduate Student Member, IEEE) received the B.Sc. and M.Sc. degrees in electronics and information technology from Johannes Kepler University, Linz, Austria, in 2017 and 2020, respectively.

During his studies, he focused on high-frequency systems and radar while completing his master's thesis about the design, simulation, and test of a fully functional FMCW—MIMO radar system with nonuniform arrays and substrate integrated waveguides. In 2020, he joined the Institute for Communication and Navigation, German Aerospace Center, Wessling, Germany, where he works on miniaturized dielectric resonator antennas, arrays, and methods for array decoupling with a focus on satellite navigation applications. In 2021, he became an external Ph.D. Student with the Microwave Sensing, Signals, and Systems Group, TU Delft, Delft, The Netherlands. In his Ph.D. project, he explores the potential of additive manufacturing with respect to high-frequency components and antenna systems.

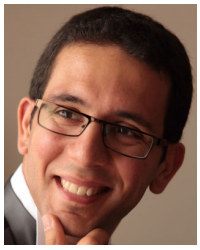

Stefano Caizzone (Member, IEEE) received the M.Sc. degree in telecommunications engineering and the Ph.D. degree in geoinformation from the University of Rome Tor Vergata, Rome, Italy, in 2009 and 2015, respectively.

Since 2010, he has been with the Antenna Group, German Aerospace Center (DLR), Wessling, Germany, where he has been responsible for the development of innovative miniaturized antennas. Since July 2020, he leads the Antenna Systems Group. His main research interests concern small antennas for satellite navigation, controlled radiation pattern antennas for robust satellite navigation and high-performance antenna design for precise satellite navigation, antenna arrays for satellite communication, and installed performance analysis.

Stefan Thurner embarked on a successful career as a Senior Flight Radar Security Officer. After creating his own business as a TV and radio technician, he completed the education to be a state-certified technician. He joined the Specialist Group Signatures with the Microwaves and Radar Institute, German Aerospace Center, Wessling, Germany, in 2002, where he is responsible for the Material Measurement Laboratory.

Alexander G. Yarovoy (Fellow, IEEE) received the diploma degree (Hons.) in radiophysics and electronics and the Candidate Phys. and Math. Sci. and Doctor Phys. and Math. Sci. degrees in radiophysics from Kharkov State University, Kharkiv, Ukraine, in 1984, 1987, and 1994, respectively.

In 1987, he joined the Department of Radiophysics, Kharkov State University, as a Researcher and became a Full Professor in 1997. From September 1994 to 1996, he was with the Technical University of Ilmenau, Ilmenau, Germany, as a Visiting Researcher. Since 1999, he has been with the Delft University of Technology, Delft, The Netherlands. Since 2009, he leads there a Chair of Microwave Sensing, Systems and Signals. His main research interests are in high-resolution radar, microwave imaging, and applied EMs (in particular, UWB antennas). He has authored and coauthored more than 500 scientific or technical articles, seven patents, and 14 book chapters. He was a recipient of the European Microwave Week Radar Award for the paper that best advances the state-of-the-art in radar technology in 2001 (together with L.P. Ligthart and P. van Genderen) and in 2012 (together with T. Savelyev). In 2010 together with D. Caratelli, he got the best paper award of the Applied Computational Electromagnetic Society (ACES).

Prof. Yarovoy served as a General TPC Chair for the 2020 European Microwave Week (EuMW'20), as the Chair and the TPC Chair for the 5th European Radar Conference (EuRAD'08), and the Secretary for the 1st European Radar Conference (EuRAD'04). He served also as the Co-Chair and TPC Chair for the Xth International Conference on GPR (GPR2004). He serves as an Associate editor for the IEEE TRANSACTION ON RADAR SYSTEMS. From 2011 to 2018, he served as an Associate Editor for the *International Journal of Microwave and Wireless Technologies*. From 2008 to 2017, he served as the Director for the European Microwave Association (EuMA).